Key Points:
- The thermosphere cools most rapidly following periods of strong auroral heating
- Nitric oxide emissions have high correlations with the heating and temperature
- Accounting for cooling by nitric acid is required for accurate model predictions

Correspondence to:
D. R. Weimer,
dweimer@vt.edu

High correlations between temperature and nitric oxide in the thermosphere

D. R. Weimer[1,2], M. G. Mlynczak[3], L. A. Hunt[4], and W. Kent Tobiska[5]

[1]Center for Space Science and Engineering Research, Virginia Polytechnic Institute and State University, Blacksburg, Virginia, USA, [2]National Institute of Aerospace, Hampton, Virginia, USA, [3]Science Directorate, NASA Langley Research Center, Hampton, Virginia, USA, [4]Science Systems and Applications, Inc., Hampton, Virginia, USA, [5]Space Environment Technologies, Pacific Palisades, California, USA

Abstract Obtaining accurate predictions of the neutral density in the thermosphere has been a long-standing problem. During geomagnetic storms the auroral heating in the polar ionospheres quickly raises the temperature of the thermosphere, resulting in higher neutral densities that exert a greater drag force on objects in low Earth orbit. Rapid increases and decreases in the temperature and density may occur within a couple days. A key parameter in the thermosphere is the total amount of nitric oxide (NO). The production of NO is accelerated by the auroral heating, and since NO is an efficient radiator of thermal energy, higher concentrations of this molecule accelerate the rate at which the thermosphere cools. This paper describes an improved technique that calculates changes in the global temperature of the thermosphere. Starting from an empirical model of the Poynting flux into the ionosphere, a set of differential equations derives the minimum, global value of the exospheric temperature, which can be used in a neutral density model to calculate the global values. The relative variations in NO content are used to obtain more accurate cooling rates. Comparisons with the global rate of NO emissions that are measured with the Sounding of the Atmosphere using Broadband Emission Radiometry instrument show that there is very good agreement with the predicted values. The NO emissions correlate highly with the total auroral heating that has been integrated over time. We also show that the NO emissions are highly correlated with thermospheric temperature, as well as indices of solar extreme ultraviolet radiation.

1. Introduction

The heat energy that is dissipated by auroral currents has a significant influence on variations in the neutral density and temperature in the thermosphere. The flux of solar ultraviolet radiation is the dominant source of the heating of the thermosphere when geomagnetic activity is low [*Tobiska et al., 2008*]; at times of high activity the more important component is the additional energy that is dissipated by the high-latitude electric fields and currents. This energy source is driven by the solar wind and interplanetary magnetic field (IMF) that originate from the sun. At times of moderate driving the ionospheric heating in both hemispheres totals several hundred gigawatts (GW) [*Chun et al.*, 1999, 2002; *McHarg et al., 2005*]. During large geomagnetic storms the auroral heating may exceed a thousand GW, resulting in neutral density changes that increase the drag on objects in low Earth orbit, to the extent that orbit prediction and tracking becomes difficult [*Lu et al.*, 1998; *Prölss, 2011*; *Weimer et al., 2011*].

Over the past few decades it has become apparent that the amount of nitric oxide (NO) in the thermosphere has a significant influence on the neutral temperature and density. The chemical reactions that produce NO have a strong temperature dependence [*Kockarts, 1980*; *Bailey et al.*, 2002; *Barth et al., 2009*; *Barth, 2010*], so that heating within the ionosphere enhances the level of NO in the lower thermosphere. Due to the sensitivity of NO production to temperature, high-latitude Joule heating has a significant role, as noted by *Barth* [2010] and others. Auroral electron precipitation also has a significant role in NO production, mainly by increasing the number density of N(^{2}D) and N(^{4}S) atoms in the lower thermosphere, which react with oxygen molecules to produce NO [*Siskind et al., 1989*; *Sætre et al., 2007*; *Barth et al., 2003*]. It has been shown by *Wilson et al.* [2006] that the total energy deposited by the electrons tends to vary in proportion to the total Joule heating. The ratio of Joule/Particle heating in the events studied ranged from 1.7 to 6.9, with a mean value of 2.8. At low latitudes, particularly when geomagnetic activity is low, soft X-ray radiation from the Sun is the primary source of NO production [*Barth et al., 1988*].

It is known that optical emissions from nitric oxide are efficient in cooling the thermosphere [_Kockarts_, 1980; _Sharma et al._, 1996; _Duff et al._, 2003]. The result is that NO acts as a self-regulating, "natural thermostat" for the thermosphere that reduces the effects of the auroral disturbances [_Mlynczak et al._, 2003, 2005].

_Lu et al._ [2010] had examined the relationship between global Joule heating and global radiative cooling emissions due to NO. Two models were coupled together in their study to derive the Joule heating energy input as well as model the NO energy output, during six geomagnetic storm periods. First-principle numerical simulations from the thermosphere ionosphere electrodynamic general circulation model [_Richmond et al._, 1992] were coupled with the assimilative mapping of ionospheric electrodynamics (AMIE) data assimilation algorithm [_Richmond_, 1992]. Both models were developed at the National Center for Atmospheric Research (NCAR). The numerical results were compared with measurements of optical emissions from NO, obtained at a wavelength of 5.3 μm by the Sounding of the Atmosphere using Broadband Emission Radiometry (SABER) instrument on the Thermosphere Ionosphere Mesosphere Energetics and Dynamics (TIMED) spacecraft. They found strong correlations between the global NO power and time-lagged Joule heating during the selected events. _Lu et al._ [2010] used their results to derive a predictive formula for the NO cooling power, based on the $F_{10.7}$ and Kp indices. Another formula had used solar irradiance measurements from the Solar EUV Experiment, also on the TIMED satellite, rather than the $F_{10.7}$ flux. Compared with the SABER measurements, these prediction formulas had correlation coefficients 0.89 and 0.90.

Weimer et al. [2011] computed the total Poynting flux into the northern and southern polar regions with an empirical model and compared these results with changes in the global exospheric temperatures. These temperatures were derived from neutral density measurements on the Challenging Mini-satellite Payload (CHAMP) and Gravity Recovery and Climate Experiment (GRACE) satellites [_Tapley et al._, 2004; _Bruinsma et al._, 2004], as described in greater detail in section 3. A differential equation was developed for calculating changes in the global exospheric temperature as a function of time. The formula required only the total Poynting flux into the ionosphere, derived from IMF measurements. The ionospheric heating increases the temperature of the thermosphere, and in the absence of further heating the temperature decreases at an exponential rate.

It was found that the exponential cooling rate was not always the same. Following time periods that had high levels of ionospheric heating and greater temperature increases, the thermosphere was observed to cool off faster than when the heating levels were more moderate. In order to obtain consistently good results in matching the differential equation model to the CHAMP and GRACE measurements, _Weimer et al._ [2011] had used a changing exponential cooling rate for the temperatures, as described later. An additional variable was added to the equations, which increased in proportion to the amount of heating and decreased when heating was absent. This variable lowered the value of the exponential time constant, resulting in a more rapid cooling of the thermosphere. All factors in the equations were derived by an automated, iterative fit to the density measurements.

The enhanced thermosphere cooling was assumed to be due to enhancements in the concentration of nitric oxide, but this conjecture was not proven at the time. One purpose of this paper is to verify the results obtained by _Weimer et al._ [2011], through a comparison to measurements of the NO emissions from the SABER instrument. Second, on the basis of new information provided by this comparison, the thermosphere temperature calculation has been improved. These results presented here lead to a capability for better predictions of neutral density. A third objective of this paper is to demonstrate exactly how sensitive the nitric oxide levels are to auroral heating and the thermospheric temperature and show their high level of correlation over long time periods.

2. Nitric Oxide Emissions Measured With SABER

The SABER instrument is a broadband radiometer that measures infrared radiance in 10 bands between 1.27 and 15 μm. Emissions from carbon dioxide (CO_2) are measured in addition to the NO. The instrument scans the Earth's limb from approximately 400 km tangent altitude down to the surface, recording an infrared radiance sample every 0.4 km. Approximately 1400 profiles of infrared emission are obtained for each of the 10 SABER channels in 1 day. The nominal instantaneous field of view of the instrument is 2 km at the tangent point on the Earth's limb.

The measured radiances are converted to volumetric emission rates in W m^{-3}, and each scan is then integrated vertically giving fluxes of power in W m^{-2}. The fluxes for each day are integrated in latitude and longitude to
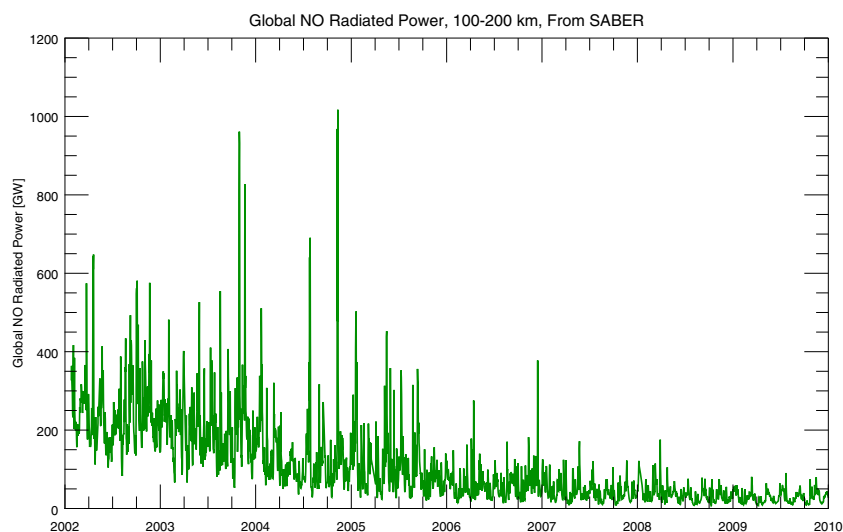
Figure 1. Global radiated power due to nitric oxide, measured with the SABER instrument. The daily mean radiative power integrated over 100 – 200 km, in units of gigawatts (GW), is shown for years 2002 through 2009.

give a daily global power emitted by the entire atmosphere, in watts. Further details about the instrument and the data processing procedures are provided by *Mlynczak et al.* [2005, 2010].

A standard data product provided by the SABER science team is a text file that provides the total global power radiated by NO and CO_2 on a daily basis. Figure 1 shows the daily power from NO for 8 years of data, from 2002 to 2010. As is evident in this figure, the radiated power follows the solar cycle, with the declining phase of solar cycle 23 evident, in addition to approximately 27 day activity variations due to solar rotation. Even more apparent are large increases in radiative power at the times of large geomagnetic storms.

While the total power of the CO_2 emissions greatly exceeds that of the NO emissions, as illustrated by *Mlynczak et al.* [2010], they come from a region that is mainly at or below the base of thermosphere, and they are not as sensitive to variations in the solar cycle and solar activity. The CO_2 cooling rates are not included in the work described here because they have a strong semiannual variation that has no correlation with the NO cooling or geomagnetic activity.

3. Prior Results From an Empirical Model

As mentioned in section 1, *Weimer et al.* [2011] had compared heating in the polar regions with changes in the global exospheric temperatures that were obtained from the CHAMP and GRACE satellites. The total Poynting flux into both hemispheres was calculated with the method described by *Weimer* [2005a], using for input values the IMF and solar wind measurements from NASAs Advanced Composition Explorer (ACE) satellite. The Magnetic Field Instrument [*Smith et al., 1998*] provided the IMF, while the solar wind velocity and number density are from the Solar Wind Electron, Proton, and Alpha Monitor instrument [*McComas et al.*, 1998]. The "level 2" data from the NASA archives are used, available at ftp://cdaweb.gsfc.nasa.gov/pub/data/ace.

The most recent version of the model described by *Weimer* [2005b] was used, referenced here on as the W05 model. The Poynting flux is derived from the electric potential and field-aligned current mappings in this model, which provide both the electric field and magnetic field perturbations above the ionosphere. This method does not depend on any model of the ionospheric conductivity, as the conductivity variations, as a function of dipole tilt angle and location, are implicitly included in the measurements used for the model's development.

The total Poynting flux flowing into both polar hemispheres as a function of time was compared with measurements of neutral densities in the thermosphere at two altitudes, obtained from accelerometers on the CHAMP and GRACE-A satellites. The derivations of the density data used in the calculations are described by

Sutton et al. [2007] and were obtained from an online database (http://sisko.colorado.edu/sutton/data.html) at the University of Colorado. File versions 2.2 are used.

The Jacchia-Bowman 2008 (JB2008) thermospheric density model [*Bowman et al.*, 2008] was used to convert the neutral density values to a measurement of thermosphere temperature. This model derives all global densities from a parameter that *Jacchia* [1970] refers to as the "global nighttime minimum exospheric temperature," and referred to as T_c. The same notation was employed by *Bowman et al.* [2008] and is also used here for continuity rather than the more descriptive symbol $T_{\infty\ min}$. In the JB2008 model, the maximum exospheric temperature on the dayside is always 1.3 times the value of the minimum, T_c.

Daily values of T_c in JB2008 are obtained from indices of solar radiation using this formula:

$$T_c = 392.4 + 3.227\bar{F}_S + 0.298\Delta F_{10} + 2.259\Delta S_{10} + 0.312\Delta M_{10} + 0.178\Delta Y_{10} \tag{1}$$

where F_{10} is a proxy index for the 10.7 cm solar radio flux. The symbols S_{10} and M_{10} represent proxy indices for the extreme ultraviolet (EUV) flux measured on the SOHO satellite and the medium ultraviolet flux from NOAA satellites. The Y_{10} index is a weighted mixture of X-ray and Lyman-α, with the X-ray measurements, at wavelengths of 0.1–0.8 nm, coming from a spectrometer instrument on the GOES satellite, and Lyman-α from the TIMED satellite. The derivation of these indices, as well as documentation of the data sources, is described by *Tobiska et al.* [2008]. The shortened notation used here follows from the same convention employed by *Bowman et al.* [2008]. The delta values in (1) represent the difference of the daily and 81 day centered, boxcar average value of each index, and $\bar{F}_S$ is obtained from a weighted combination of the running-average values of F_{10} and S_{10}.

More rapid changes to the T_c temperature, due to the auroral heating associated with geomagnetic activity, are referred to as ΔT_c. In the JB2008 model hourly values of the ΔT_c correction are calculated from the *Dst* index, using the formula by *Burke* [2008].

Weimer et al. [2011] had developed a method to derive measurements of ΔT_c from the CHAMP and GRACE data, using the JB2008 model in reverse, to find the temperature value that produced a match with the measured neutral densities. The orbit-averaged values of this ΔT_c from the two satellites were in very close agreement, even though they are at different altitudes and often in different orbit planes. It was found that ΔT_c could be predicted very well from the Poynting flux in the W05 model with this formula:

$$\Delta T_c(t_{n+1}) = \Delta T_c(t_n) - \Delta T_c(t_n)(\Delta t/\tau_c) + \alpha H_J(t_n)\Delta t \tag{2}$$

$$\Delta NO(t_{n+1}) = \Delta NO(t_n) - \Delta NO(t_n)(\Delta t/\tau_{NO}) + \beta H_J(t_n)\Delta t \tag{3}$$

$$\tau_c = 14.6\ (h) - 0.281\ NO \tag{4}$$

The H_J in this formula is the total Joule heating from the W05 model in both hemispheres, and α is a scaling factor that relates the temperature increases to the heating input within each time step, having a value of $6.9 \cdot 10^{-4}$ K/(GW min) or $1.2 \cdot 10^{-5}$ K/GJ. The exponential cooling rate of the thermosphere is τ_c, and ΔNO represents the changes in nitric oxide concentration, using an arbitrary scaling that has no physical units assigned. Equation (3) causes this ΔNO level to increase in proportion to the heating, with scaling factor β, and decay with an exponential time constant $\tau_{NO} = 28.0$ h. The value of β was preset to a value that increased the level of ΔNO by 0.0001 for each GW of heating, in every 4 min time step. As equation (4) shows, as the level of ΔNO increases, then the time constant τ_c for the thermosphere cooling rate becomes smaller, resulting in a more rapid exponential decay of the temperature.

The values of all constants other than β were determined by fitting the calculated values of ΔT_c to the values that were derived from the CHAMP and GRACE density measurements. All data from the years 2003 through 2005 were used for this least error fit. The "downhill, simplex" method described by *Press et al.* [1986] was used in a program that reiteratively adjusts all variables until a minimum value of the error is reached, to within the limits of assigned tolerance values. A modification to their original "Amoeba" program was made such that the tolerance is specified as a vector rather than a scalar.
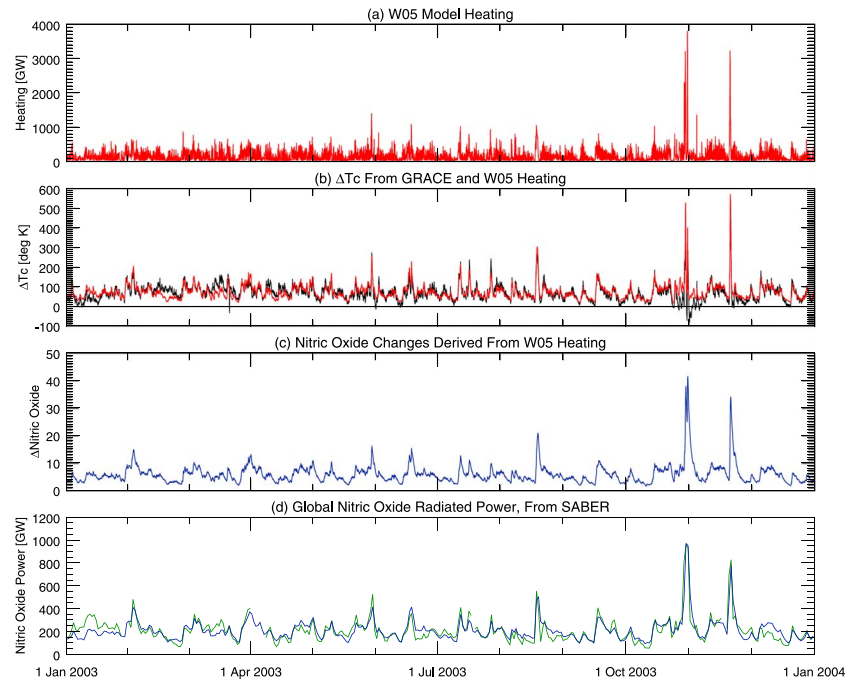
Figure 2. Results from the thermosphere temperature calculation described by *Weimer et al.* [2011], for 2003. (a) The total auroral heating, in GW, calculated from the W05 empirical model. (b) Black line shows the ΔT_c parameter derived from neutral density measurements on the GRACE satellite. The red line shows ΔT_c that are derived from the heating, using equations (2)–(4). (c) The blue line shows a variable that is proportional to changes in global NO levels, from (3). These are calculated at 4 min time steps. (d) The green line shows the SABER NO power measurements. The superposed blue line shows the linear fit of the values shown in Figure 2c, after 24 h smoothing, from equation (6).

One other adjustment was required in order to obtain the best fit, that being an additional saturation factor for the total heating from the W05 model. The ionospheric electric potentials are known to increase, then roll-off to a nearly flat slope, as the magnitude of the interplanetary electric field increases [*Siscoe et al., 2004*]. Even though this model already had some saturation built in, there were no data at sufficiently high driving levels to fully resolve the roll-off of the electric potentials at large IMF magnitudes. In this study it was found that an additional, nonlinear reduction in heating at high driving levels was needed in order to produce good fits at both low and high levels of heating, otherwise the calculated temperatures were too large in the more extreme events. This additional saturation was provided by

$$J_H = J_{W05} \frac{1 + \frac{500}{3900}}{1. + \frac{J_{W05}}{3900}} \tag{5}$$

which maintains a nearly linear curve with slope of 1 up to 500 GW before the roll-off toward saturation. This saturation curve is applied separately for each hemisphere's total heating. The value of 3900 that produced the best fit was found with a reiterative process.

An example of the results from the ΔT_c calculation in (2)–(5) is shown in Figure 2 for the entire year 2003. The red line in Figure 2a shows the total heating from the W05 model that is calculated from the ACE measurements in the solar wind, while the red line in Figure 2b shows the ΔT_c values that are calculated. The superposed black line in Figure 2b shows the ΔT_c values derived from the GRACE density measurements. For the majority of the time these two curves are in good agreement, with the most obvious difference being at the end of October 2003, during the well-known "Halloween Storm". In this event the thermosphere had cooled so rapidly that the measured value of ΔT_c went negative, meaning that the temperature went below the more slowly varying value of T_c derived from the solar indices by application of (1). This rapid cooling phenomenon during this event has previously been noted by *Weimer et al.* [2011] and *Lei et al.* [2012].

The value of the ΔNO variable calculated with (3) is illustrated with the blue line in Figure 2c. For comparison, the SABER measurements of the NO radiated power during this time period are shown in Figure 2d with

the green line. These data are the same as shown in Figure 1. For an easier comparison the values of ΔNO computed at 4 min intervals have been smoothed to the same 24 h cadence of the SABER data and fit to the measurements. The blue line in Figure 2d shows the result of the fit, with the linear equation

$$NO_{SABER} = 33 + 29 \, \Delta NO_3 \tag{6}$$

ΔNO_3 refers to the values computed with (3), and the correlation with NO_{SABER} is 0.88, with a mean error (absolute deviation) of 38 GW and a standard deviation of 53 GW. Higher correlations were obtained in other years.

4. Improving the Thermosphere Temperature Prediction

While equations (2)–(4) do a good job of modeling the temperature perturbations that were derived from the density measurements, there is one deficiency in that the ΔT_c value from (2) cannot be negative. On the other hand, the measured values of ΔT_c do have negative values during the October 2003 geomagnetic storm. This discrepancy causes some inaccuracy in the results in situations where accuracy is needed the most.

The comparison with the SABER measurements confirms that the NO radiated power does indeed increase in proportion to the total auroral heating. This validation, coupled with a desire to obtain ΔT_c values that can be negative, leads to the realization that the calculation could be modified so that an increase in the level of NO leads to a direct reduction in the temperature due to radiated power rather than an ad hoc reduction in the cooling time constant. The revised equation for calculating ΔT_c is

$$\Delta T_c(t_{n+1}) = \Delta T_c(t_n) - \Delta T_c(t_n)\left(\frac{\Delta t}{\tau_c}\right) + \alpha H_J(t_n)\,\Delta t - C_{NO}(t_n)\Delta t \tag{7}$$

In this equation C_{NO} represents cooling from the nitric oxide that contributes to a temperature reduction in each time step, while the fixed time constant τ_c controls the exponential decay due to heat conduction and other radiative species. If the value of ΔT_c at time step t_n does become negative, then the second term, with the time constant τ_c, on the right side of (7) is not included. The value of a dimensionless quantity ΔNO with arbitrary scaling is calculated from the heating as before:

$$\Delta NO(t_{n+1}) = \Delta NO(t_n) - \Delta NO(t_n)\left(\frac{\Delta t}{\tau_{NO}}\right) + \beta H_J(t_n)\,\Delta t \tag{8}$$

As in the previous equation, the value of β was preset to a value that increased the level of ΔNO by 0.0001 times the total heating in GW, in every 4 min time step.

The value of C_{NO} is proportional to the value of ΔNO from (8) times the total temperature, minus an offset:

$$C_{NO}(t_n) = \gamma \Delta NO(t_n)(T_{Solar}(t_n) + \Delta T_c(t_n) - \varepsilon) \tag{9}$$

T_{Solar} represents the variations in the exospheric temperature due to solar radiation, as calculated with (1). It is noted that how ΔNO is used in (9) is quite different from how it acts in (4); this symbol represents a different quantity.

The variables in these equations were derived from a least error fit with the ΔT_c values that were obtained from the GRACE neutral density measurements over a 3 year time span. As before, the downhill, simplex method [*Press et al.*, 1986] was used for the fit. The revised fitting process now included a simultaneous adjustment of the saturation curve in (5), increasing the number of variable parameters to six. Since the downhill method requires an initial starting guess for the solution, it was helpful to first narrow down the approximate location of the solution in the six-dimensional space, through a trial of all combinations on a coarse grid. The CHAMP data were not used in this fit, due to some concerns about the precision of the drag calibrations.

The result of the new fit with equations (7)–(9) was $\alpha = 7.08 \cdot 10^{-4}$ K/(GW min) ($1.2 \cdot 10^{-5}$ K/GJ), $\tau_c = 16.3$ h, $\gamma = 3.95 \cdot 10^{-5}$/min, $\tau_{NO} = 14.9$ h, and $\varepsilon = 544°$K. The revised heating saturation curve had 1560 in (5), rather than 3900, resulting in a greater reduction in the heating at high driving levels.
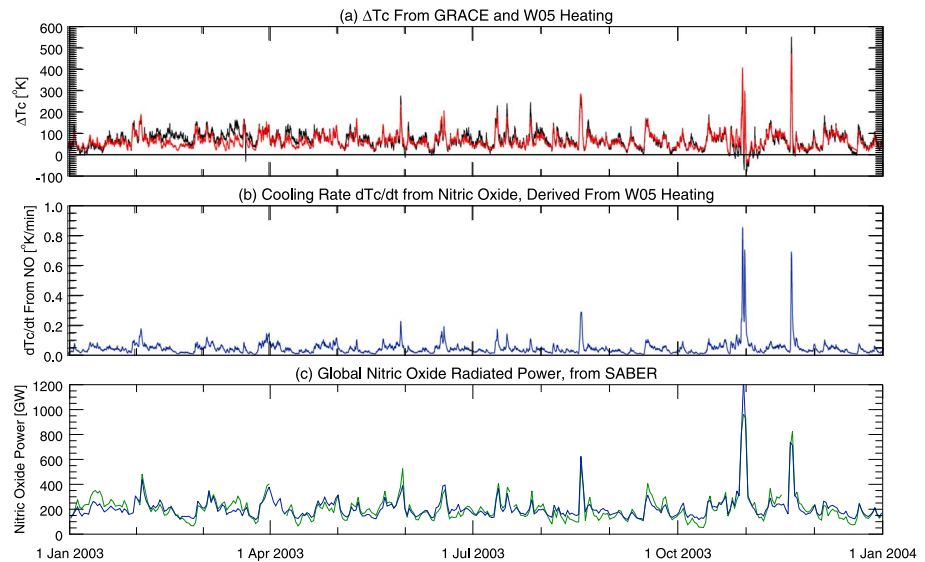
Figure 3. Results from the revised thermosphere temperature calculation described here for the year 2003. (a) Values of the ΔT_c parameter that were derived from the neutral density measurements on the GRACE satellite are shown in black, the same values as shown in Figure 2b. The red line shows these values that are derived from the global heating, using equations (7)–(9). (b) The blue line shows the cooling rate of the thermosphere that is proportional to changes in global NO levels, times the temperature, from (9). These are calculated at 4 min time steps. (c) Like Figure 2d, the green line shows the SABER NO power measurements, while the superposed blue line shows the linear fit of the same values shown in Figure 3b, using (10).

Figure 3 shows the result of the new ΔT_c calculations for the same time span as shown in Figure 2. As the heating from the W05 model is exactly the same, it is not included in this graph. The plot in Figure 3a has the ΔT_c levels from GRACE in black and equation (7) superposed in red. The agreement between the two has improved in the October–November 2003 geomagnetic storm periods, particularly where the GRACE data indicate that ΔT_c should be negative.

Figure 3b shows the value of C_{NO} with the blue line, at the 4 min cadence. The levels are different from Figure 2 since the values that are plotted are from (9) rather than (3). This quantity indicates the rate of change in temperature per time step, due to the NO cooling, in units of K/min. The line in Figure 3b shows the results at the original, 4 min time steps. Figure 3c shows the comparison with the daily, NO emissions measured on SABER (green line). The blue line shows the result of a linear fit, after smoothing Figure 3b to the same 24 h intervals used for the SABER measurements:

$$NO_{SABER} = 92 + 2370 \, C_{NO} \tag{10}$$

The correlation has increased to 0.92, even though no SABER measurements were used in the fitting process. As the revised fit resulted in a smaller time constant τ_{NO}, the blue line drops faster than before. A close comparison of the graphs indicates that the faster decay has a better match with the SABER measurements. The mean error is lower as well, at 34 GW, and the standard deviation is 43 GW. While the values shown in Figure 3b seem small, a value of 0.6 K/min amounts to a temperature change of 430°K if sustained over a 12 h period.

Figure 4 shows a similar comparison between the derived value of C_{NO} and the measured NO emissions, over a 4 year period. In Figure 4a the values of C_{NO} are shown with the 24 h averaging already calculated so that the heights of the peak values are less than in Figure 3. The plot in Figure 4b again shows the SABER measurements of NO emissions (green line) and the linear fit with the data from Figure 4a (blue line). Over this 4 year period the formula for best fit is

$$NO_{SABER} = 42 + 2790 \, C_{NO} \tag{11}$$

The correlations between the two values is still 0.92 for this entire, 4 year period, and the mean error is 30 GW, with a standard deviation of 41 GW. Both the declining phase of the solar cycle as well as the periodicity of the 27 day solar rotation are evident in Figure 4.
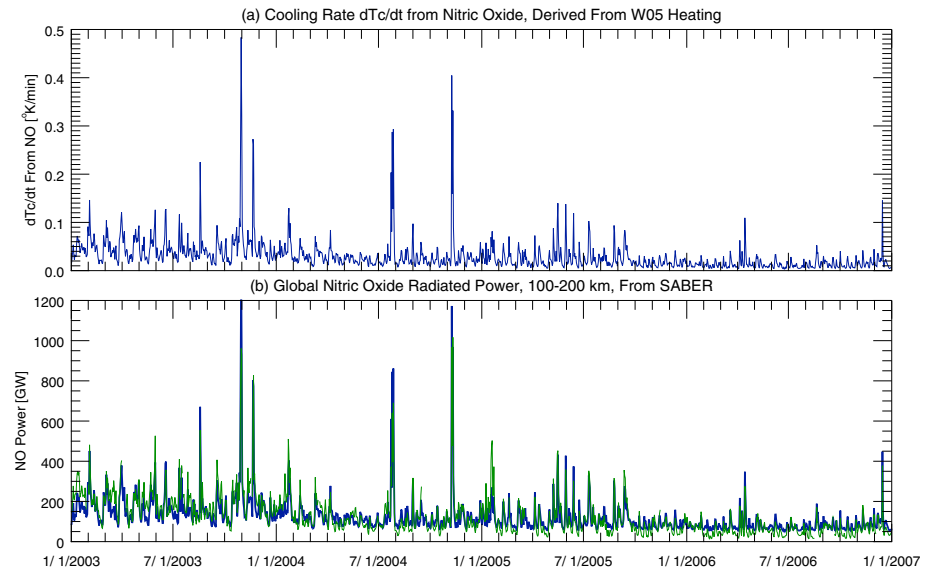
Figure 4. Results from the revised thermosphere temperature calculation described here for the years 2003 through 2006. (a) The blue line shows the cooling rate of the thermosphere due to the effect of NO. These are the same as in Figure 3c, except the longer time period is shown and the 24 h smoothing has already been applied. (b) The green and blue lines are the same as in Figure 3c, using the fit in equation (11) for this longer time interval.

5. Nitric Oxide Emissions Compared With Thermosphere Temperatures

The previous section has compared the measured nitric oxide emissions with variables that are derived from the global heating rates. It is useful to make another comparison directly with the thermosphere temperature rather than the NO parameter derived from equations (3) or (9). Figure 5 shows one such comparison for the years 2003 through 2006. In the upper graph Figure 5a the thicker, dark-red line shows the value of T_c calculated from solar indices with (1), as used in the JB2008 model. The thinner, red line shows this value with the addition of the ΔT_c values, from (7), giving the total temperature. The maximum value of this temperature
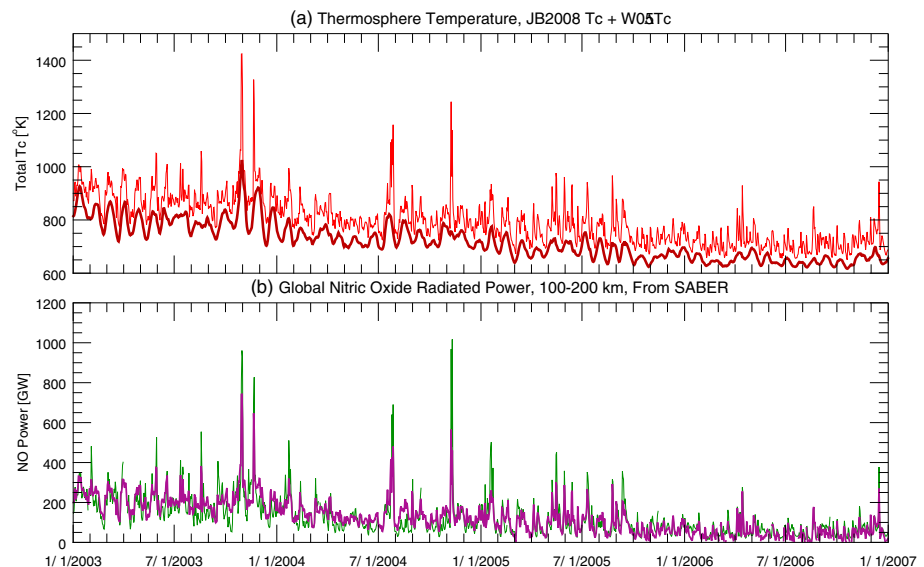

Figure 5. Comparison of the NO emissions measured with SABER and the temperature of the thermosphere. (a) The thicker, dark red line shows the T_c parameter used in the JB2008 model, as calculated with (1). The lighter red line shows the sum of this T_c plus the ΔT_c values that were calculated with (7). The largest temperature values in each 24 h period are used. (b) Green line shows the SABER measurements of NO emissions, and the purple line shows the linear fit of the total temperature, from (12).
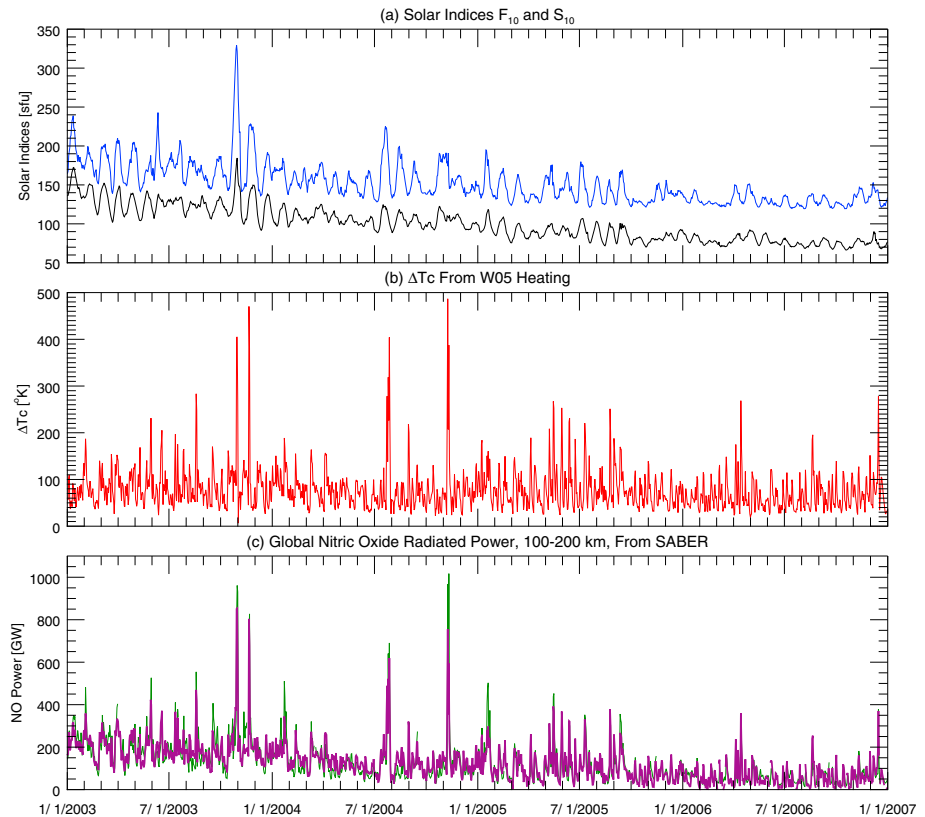
Figure 6. Comparison of the NO emissions measured with SABER with solar indices F_{10} and S_{10} and the temperature of the thermosphere. (a) Blue line shows the F_{10} index, offset by 50 sfu, and the black line shows the S_{10} index. (b) The red line shows the ΔT_c values that were calculated with (7). (c) As in the other graphs, the green line shows the SABER measurements of NO emissions, and the purple line shows the multiple linear regression fit of the other three values from (13).

in each day is used here. As in the earlier graphs, Figure 5b shows the SABER measurements with a green line, and a superposed line shows a linear fit of the total temperature:

$$NO_{SABER} = -659 + .984(T_c + \Delta T_c) \tag{12}$$

For clarity, a purple line is used to show the temperature in this plot. The correlation between the measured NO emission and the total temperature is 0.87, the mean error is 35 GW, and the standard deviation is 51 GW. The mean value of the temperature in each day had been tried for comparison, rather than the maximum value, and this resulted in lower correlation with the NO emissions.

While this comparison of the NO emissions with the total T_c has a good correlation, it led to a question about whether an agreement could be found with a more simple calculation from the solar indices. The formula in (1) requires calculation of an 81 day centered, boxcar average of these indices, which is not possible in real time. Using a multiple linear regression with indices having various smoothing lengths and delays, it was found that the best correlation with the NO emissions is found with

$$NO_{SABER} = -217 + 1.46\,\Delta T_c + 0.831\,F_{10} + 2.33\,S_{10} - 0.634\,M_{10} - 0.221\,Y_{10} \tag{13}$$

The correlation coefficient is 0.904, the mean error is 30.7 GW, and the standard deviation is 43.9 GW. As before, the maximum value of ΔT_c in each 24 h is used for the comparison with the 24 h NO_{SABER} values. This correlation was achieved using a 3 day centered, boxcar that is time shifted by 1 day, for all solar indices. In other words, the solar indices are their mean value from the current day and prior 2 days.

If only the F_{10} and S_{10} indices are used in the regression, then there is only a minuscule reduction in the correlation, to 0.903, with the same smoothing and delay. The revised formula is

$$NO_{SABER} = -217 + 1.47\,\Delta T_c + 0.656\,F_{10} + 1.62\,S_{10} \tag{14}$$

There is only a small change in the mean error, to 30.8 GW, with a standard deviation of 44.1 GW. In other words, the changes are insignificant; the reason being that these indices tend to be strongly correlated with each other. Figure 6 shows the comparison of the solar indices with the SABER measurements, using (14) to generate the purple line in Figure 6c. Figure 6a shows the F_{10} and S_{10} indices, drawn with the blue and black lines, with F_{10} offset by +50 solar flux unit (sfu) for better clarity.

6. Discussion

In the previous work by *Weimer et al.* [2011] a method had been developed to derive predictions of the thermospheric temperature, using the total auroral heating in the polar regions, as summarized in equations (2)–(4). A dimensionless variable had been included in order to account for variations in the rate of cooling in the thermosphere, as observed with the neutral density measurements from CHAMP and GRACE. The more rapid cooling that followed increased levels of heating was attributed to nitric oxide production. This link was not proven at the time, and this follow-up comparison with the measurements from the SABER instrument, as illustrated in Figure 2, shows a very good correlation, 0.88, for 2003.

In this follow-up work, in addition to showing convincing evidence that nitric oxide is indeed responsible for enhanced thermosphere cooling, an improved formula is shown. The main shortcoming of the earlier method was that the corrections to the temperature T_c in the JB2008 model could not go below zero, while observations indicated that the actual temperature could go below the baseline level, following extreme geomagnetic activity.

The revised formula is provided in equations (7) through (9). Figure 3 shows that this new temperature correction calculation did go below zero following the 2003 Halloween storm, resulting in a better agreement with the neutral density measurements. The variable that represents NO in the new formula has a more direct relationship with the power level of the cooling, NO emissions, and this power has a higher correlation with the measured emissions, 0.92, for 2003. For a 4 year period the correlation is also 0.92, as illustrated in Figure 4. This level of correlation is quite amazing, in consideration that one quantity is from the optical measurements of NO emissions, and the other is derived entirely independently: solar wind and IMF measurements were passed through an empirical model and processed with simple differential equations that use scaling factors and time constants that were derived by fitting neutral density measurements.

As mentioned in the previous paper, the thermosphere behaves like a calorimeter, such that for a specified change in temperature the amount of energy involved can be estimated. The calculations by *Burke* [2008] with the Jacchia 1977 model indicated that raising T_c or $T_{\infty\,min}$ by 1°K increases the total energy in the thermosphere above 100 km altitude by $1.01 \cdot 10^{14}$ J. Therefore, a specified change in the global thermosphere temperature is related to the total amount of thermal and potential energy within the system.

It was stated that using $\alpha = 7.08 \cdot 10^{-4}$ K/(GW min), or ,$1.2 \cdot 10^{-5}$ K/GJ, in (7) produced the best agreement with the neutral density measurements from GRACE. This number indicates that a heating level of 1410 GW in the model is needed to raise T_c temperature by 1°K in 1 min, increasing the total energy by $1.01 \cdot 10^{14}$ J. A heat dissipation of 1410 GW over 1 min produces $8.47 \cdot 10^{13}$ J, which is about 80% of the *Burke* [2008] calculation. The auroral particle precipitation can add another 20% or more to what the W05 model calculates [*Wilson et al.*, 2006], which can account for the missing energy.

Another way to apply the results by *Burke* [2008] is that 1 GW of heating or cooling applied over a 1 min time period should increase or decrease T_c by $5.95 \cdot 10^{-4}$ K. Referring to the fit results in (11), each GW of NO radiated power measured by SABER is proportional to 2790 times C_{NO}, in units of K/min. This results in the NO radiation measured by SABER cooling the thermosphere at $3.58 \cdot 10^{-4}$ K/min for each GW of radiated power or 61% of the theoretical value.

Figure 5 shows that the NO emissions have a good correlation (0.87) with the total thermospheric temperature, using the value of T_c derived from solar indices from (1) plus the ΔT_c calculated with (7). The maximum value of the temperature in each day had a better correlation than the mean temperature value, which is easily explained by the fact that both the peak value and NO emissions are affected by the total heating during the previous several hours. Figure 5 is also useful to illustrate how the NO emissions are influenced by the 27 day periodicity in solar radiation as well as the variation in this radiation over the solar cycle.

As mentioned in section 1, in the publication by *Lu et al.* [2010] they had discussed the correlations between the SABER NO measurements and the $F_{10.7}$ index and the flux from the Solar EUV Experiment on the TIMED satellite. In the separate comparisons, power law functions of these quantities had correlations of 0.85 and 0.82, respectively. Exponents of 0.72 and 0.59 were determined with least error fitting. The largest correlation values were found when the indices were lagged by 1 day. Time periods with geomagnetic storm enhancements were excluded. To account for storm time heating, a time-averaged value of the Kp index with an exponent of 3.1 was included in their final prediction formulas, and correlations of 0.89 and 0.90 were achieved for a 7 year period. All versions of the Mass Spectrometer Incoherent Scatter class thermosphere models [*Hedin*, 1983] also use a 1 day lag for the $F_{10.7}$ index.

These prior results were one motivation for trying the correlations shown in Figure 6, as well as desire to find a more simple alternative to (1) to predict thermosphere temperatures and to avoid the use of an 81 day boxcar average. The results illustrated in Figure 6 showed that a 0.90 correlation with the SABER measurements could be achieved using a linear combination of the ΔT_c parameter plus the F_{10} and S_{10} indices described by *Tobiska et al.* [2008]. This correlation was obtained by use of the mean value of these solar indices over 3 days, using the current and prior 2 days.

7. Summary and Conclusion

A long-standing problem has been the calculation of neutral density changes in the thermosphere following large geomagnetic storms, as well as the slower variations throughout the solar cycle. Accurate predictions of such effects have been elusive. This paper describes an improvement on a technique that calculates changes in the global, minimum temperature of the thermosphere, based on solar wind/IMF values that are passed through an empirical model of Poynting flux flowing into the polar ionospheres. This temperature can be used in the JB2008 model, or future variations, in order to derive the global neutral density values in geospace.

A key parameter in this prediction is the total amount of nitric oxide in the thermosphere. Enhanced levels of heating and particle precipitation in the ionosphere effectively increase both the temperature and the concentration of NO in the thermosphere, which in turn accelerates the rate at which the thermosphere cools. The result is that the cooling rate is not constant. Relative variations in NO content are used in the temperature calculation, using coefficients that were obtained by a repetitive, least error fit to thermosphere temperatures that were derived from neutral density measurements on the GRACE satellite. Later comparisons with the global rate of NO emissions measured with the SABER instrument on the TIMED satellite indicated that there is a very good agreement between the predicted and measured values. The NO emissions correlate highly with the total auroral heating that has been integrated over time, and they also correlate well with the temperature of the thermosphere.

References

Bailey, S. M., C. A. Barth, and S. C. Solomon (2002), A model of nitric oxide in the lower thermosphere, *J. Geophys. Res.*, *107*(A8), doi:10.1029/2001JA000258.

Barth, C. A. (2010), Joule heating and nitric oxide in the thermosphere, 2, *J. Geophys. Res.*, *115*, A10305, doi:10.1029/2010JA015565.

Barth, C. A., W. K. Tobiska, D. E. Siskind, and D. D. Cleary (1988), Solar-terrestrial coupling: Low-latitude thermospheric nitric oxide, *Geophys. Res. Lett.*, *15*, 92–94.

Barth, C. A., K. D. Mankoff, S. M. Bailey, and S. C. Solomon (2003), Global observations of nitric oxide in the thermosphere, *J. Geophys. Res.*, *108*, 1027, doi:10.1029/2002JA009458.

Barth, C. A., G. Lu, and R. G. Roble (2009), Joule heating and nitric oxide in the thermosphere, *J. Geophys. Res.*, *114*, A05301, doi:10.1029/2008JA013765.

Bowman, B. R., W. K. Tobiska, F. A. Marcos, and C. Valladares (2008), The JB2006 empirical thermospheric density model, *J. Atmos. Sol. Terr. Phys.*, *70*, 774–793.

Bruinsma, S., D. Tamagnan, and R. Biancale (2004), Atmospheric densities derived from CHAMP/STAR accelerometer observations, *Planet. Space Sci.*, *52*, 297–312.

Burke, W. J. (2008), Stormtime energy budgets of the global thermosphere, in *Mid-Latitude Ionospheric Dynamics and Disturbances, Geophys. Monogr. Ser.*, vol. 181, edited by P. M. Kintner et al., pp. 235–246, AGU, Washington, D. C.

Chun, F. K., D. J. Knipp, M. G. McHarg, G. Lu, B. A. Emery, S. Vennerstrom, and O. A. Troshichev (1999), Polar cap index as a proxy for hemispheric Joule heating, *Geophys. Res. Lett.*, *26*(8), 1101–1104.

Chun, F. K., D. J. Knipp, M. G. McHarg, J. R. Lacey, G. Lu, and B. A. Emery (2002), Joule heating patterns as a function of polar cap index, *J. Geophys. Res.*, *107*(A7), 1119, doi:10.1029/2001JA000246.

Duff, J. W., H. Dothe, and R. D. Sharma (2003), On the rate coefficient of the $N(^2D) + O_2 \rightarrow NO + O$ reaction in the terrestrial thermosphere, *Geophys. Res. Lett.*, *30*, 1259, doi:10.1029/2002GL016720.

Hedin, A. E. (1983), A revised thermospheric model based on mass spectrometer and incoherent scatter data: MSIS-83, *J. Geophys. Res.*, *88*(A12), 10,170–10,188.

Jacchia, L. G. (1970), New static models of the thermosphere and exosphere with empirical temperature profiles, *Tech. Rep. Spec. Rep. 313*, Smithsonian Astrophysical Observatory, Cambridge, U. K.

Kockarts, G. (1980), Nitric oxide cooling in the terrestrial thermosphere, *Geophys. Res. Lett.*, *7*, 137–140, doi:10.1029/GL007i002p00137.

Lei, J., A. G. Burns, J. P. Thayer, W. Wang, M. G. Mlynczak, L. A. Hunt, X. Dou, and E. Sutton (2012), Overcooling in the upper thermosphere during the recovery phase of the 2003 October storms, *J. Geophys. Res.*, *117*, A03314, doi:10.1029/2011JA016994.

Lu, G., et al. (1998), Global energy deposition during the January 1997 magnetic cloud event, *J. Geophys. Res.*, *103*(A6), 11,685–11,694.

Lu, G., M. G. Mlynczak, L. A. Hunt, T. N. Woods, and R. G. Roble (2010), On the relationship of Joule heating and nitric oxide radiative cooling in the thermosphere, *J. Geophys. Res.*, *115*, A05306, doi:10.1029/2009JA014662.

McComas, D. J., S. J. Bame, P. Barber, W. C. Feldman, J. L. Phillips, and P. Riley (1998), Solar wind electron, proton, and alpha monitor (SWEPAM) on the Advanced Composition Explorer, *Space Sci. Rev.*, *86*, 563–612.

McHarg, M., F. Chun, D. Knipp, G. Lu, B. Emery, and A. Ridley (2005), High-latitude Joule heating response to IMF inputs, *J. Geophys. Res.*, *110*, A08309, doi:10.1029/2004JA010949.

Mlynczak, M., et al. (2003), The natural thermostat of nitric oxide emission at 5.3 mm in the thermosphere observed during the solar storms of April 2002, *Geophys. Res. Lett.*, *30*(21), 2100, doi:10.1029/2003GL017693.

Mlynczak, M. G., et al. (2005), Energy transport in the thermosphere during the solar storms of April 2002, *J. Geophys. Res.*, *110*, A12S25, doi:10.1029/2005JA011141.

Mlynczak, M. G., et al. (2010), Observations of infrared radiative cooling in the thermosphere on daily to multiyear timescales from the TIMED/SABER instrument, *J. Geophys. Res.*, *115*, A03309, doi:10.1029/2009JA014713.

Press, W. H., B. P. Flannery, S. A. Teukolsky, and W. T. Vetterling (1986), *Numerical Recipes: The Art of Scientific Computing*, Cambridge Univ. Press, New York.

Prölss, G. W. (2011), Density perturbations in the upper atmosphere caused by the dissipation of solar wind energy, *Surv. Geophys.*, *32*, 101–195, doi:10.1007/s10712-010-9104-0.

Richmond, A. D. (1992), Assimilative mapping of ionospheric electrodynamics, *Adv. Space Res.*, *6*, 59–68.

Richmond, A. D., E. C. Ridley, and R. G. Roble (1992), A thermosphere/ionosphere general circulation model with coupled electrodynamics, *Geophys. Res. Lett.*, *19*(6), 601–604, doi:10.1029/92GL00401.

Sætre, C., C. A. Barth, J. Stadsnes, N. Østgaard, S. M. Bailey, D. N. Baker, G. A. Germany, and J. W. Gjerloev (2007), Thermospheric nitric oxide at higher latitudes: Model calculations with auroral energy input, *J. Geophys. Res.*, *112*, A08306, doi:10.1029/2006JA012203.

Sharma, R. D., H. Dothe, F. von Esse, V. A. Kharchenko, Y. Sun, and A. Dalgarno (1996), Production of vibrationally and rotationally excited NO in the night time terrestrial thermosphere, *J. Geophys. Res.*, *101*(A9), 19,707–19,713.

Siscoe, G., J. Raeder, and A. J. Ridley (2004), Transpolar potential saturation models compared, *J. Geophys. Res.*, *109*, A09203, doi:10.1029/2003JA010318.

Siskind, D., C. Barth, D. Evans, and R. Roble (1989), The response of thermospheric nitric oxide to an auroral storm: 2. Auroral latitudes, *J. Geophys. Res.*, *94*(A12), 899.

Smith, C. W., M. H. Acuna, L. F. Burlaga, J. L. N. F. Ness, and J. Scheifele (1998), The ACE magnetic field experiment, *Space Sci. Rev.*, *86*, 613–632.

Sutton, E. K., R. S. Nerem, and J. M. Forbes (2007), Density and winds in the thermosphere deduced from accelerometer data, *J. Spacecr. Rockets*, *44*(6), 1210–1219, doi:10.2514/1.28641.

Tapley, B. D., S. B. M. Watkins, and C. Reigber (2004), The gravity recovery and climate experiment: Mission overview and early results, *Geophys. Res. Lett*, *31*, LO9607, doi:10.1029/2004GL019929.

Tobiska, W. K., S. D. Bouwer, and B. R. Bowman (2008), The development of new solar indices for use in thermospheric density modeling, *J. Atmos. Sol. Terr. Phys.*, *70*, 803–819.

Weimer, D. R. (2005a), Improved ionospheric electrodynamic models and application to calculating Joule heating rates, *J. Geophys. Res.*, *110*, A05306, doi:10.1029/2004JA010884.

Weimer, D. R. (2005b), Predicting surface geomagnetic variations using ionospheric electrodynamic models, *J. Geophys. Res.*, *110*, A12307, doi:10.1029/2005JA011270.

Weimer, D. R., B. R. Bowman, E. K. Sutton, and W. K. Tobiska (2011), Predicting global average thermospheric temperature changes resulting from auroral heating, *J. Geophys. Res.*, *116*, A01312, doi:10.1029/2010JA015685.

Wilson, G. R., D. R. Weimer, J. O. Wise, and F. A. Marcos (2006), Response of the thermosphere to Joule heating and particle precipitation, *J. Geophys. Res.*, *111*, A10314, doi:10.1029/2005JA011274.